Comparative studies of the phase evolution in M-doped $Li_xMn_{1.5}Ni_{0.5}O_4$ (M = Co, Al, Cu and Mg) by in-situ X-ray diffraction

W. Zhu [a], D. Liu [a], J. Trottier [a], C. Gagnon [a], A. Guerfi [a], C.M. Julien [c], A. Mauger [b], K. Zaghib [a],*

[a] Energy Storage and Conversion, Research Institute of Hydro-Québec, Varennes, Québec J3X 1S1, Canada
[b] Institut de Minéralogie, de Physique des Matériaux et de Cosmochimie (IMPMC), UPMC Univ. Paris 6, 4 place Jussieu, 75005 Paris, France[1]
[c] Sorbonne Universités, UPMC Univ. Paris 6, Physicochimie des Electrolytes et Nanosystèmes Interfaciaux (PHENIX), UMR 8234, F-75005 Paris, France

HIGHLIGHTS

- Structural changes of different metal ions doped $LiMn_{1.5}Ni_{0.5}O_4$ were studied by in-situ XRD.
- Various voltage-plateau shifts for the Ni^{2+}/Ni^{4+} were found with different substitutions.
- Co-substitution was found to be promising approach with improved electrochemical property.

GRAPHICAL ABSTRACT
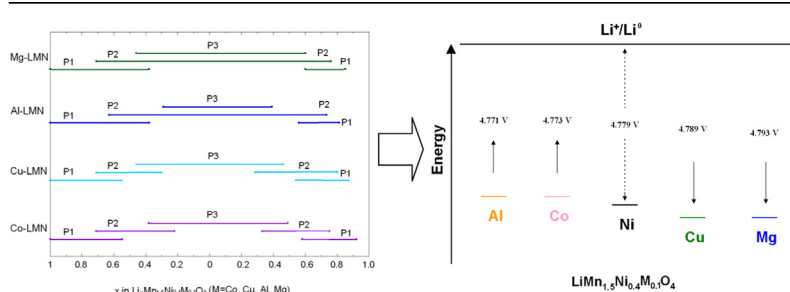
ARTICLE INFO

ABSTRACT

A series of metal-doped $LiMn_{1.5}Ni_{0.5}O_4$ (metal = Co, Al, Cu and Mg) positive electrode materials for lithium ion batteries were synthesized and their structural changes during the galvanostatic charge/discharge process at C/24 rate were investigated by using in situ X-ray diffraction (XRD) measurements. The phase diagram shows that similar series of first-order phase transitions with two regions of two-phase coexistence are observed during intercalation/de-intercalation of lithium among all the doped cathode materials. However, minor differences of the phase evolution and the electrochemical properties point to the different roles of the dopant ions. The phase diagram is analyzed and discussed, together with the differences among different results reported in the literature to distinguish between general intrinsic properties of spinel and sample-dependent properties due to the degree of cation ordering, out-of-equilibrium effects, electro-negativity and radii of the dopant ions. Among the metal-substituted samples, we argue that the Co-doping is the most promising approach with improved electrochemical property.

1. Introduction

High voltage spinel $LiMn_{1.5}Ni_{0.5}O_4$ (denoted LMN hereafter) is considered to be one of the most promising cathode materials for Li-ion batteries that can be used for hybrid electrical vehicles (HEVs) and plug-in hybrid electric vehicles (PHEVs) [1–2] due to its high voltage plateau at around 4.7 V, making its energy density (650 Wh kg^{-1}) 20% and 30% higher than that of conventional $LiCoO_2$ and $LiFePO_4$ materials, respectively [3–4]. The intrinsically fast Li^+ diffusion within the three-dimensional spinel structure leads to a good rate capability and cycling stability, making LMN attractive for vehicle applications [5–6]. However, the electro-chemical properties of LMN, especially the high-rate performance, are very sensitive to the presence of Mn^{3+} ions, cation ordering, and

oxygen vacancies, making the correlation among synthesis structure and performance a challenge [7—12]. Loss of oxygen can introduce a rock-salt impurity phase, as well as the appearance of a shoulder at around 4.0 V versus Li^+/Li^0 in the charge and discharge curves, which is indicative of the presence of Mn^{3+} in the spinel phase. The presence of an impurity rock-salt phase and a spinel phase containing Mn^{3+} is commonly observed after annealing at 800—1000 °C; ordering of the Ni^{2+} and the Mn^{4+} ions on the octahedral sites signals the presence of the stoichiometric spinel.

Two approaches have been used to improve the cycling performance and the rate capability, namely the surface coating with Li permeable oxides [13—18] and partial cation substitutions for Ni and/or Mn [19—23]. The latter approach improves the electrochemical performances and also represents a low-cost manufacturing approach compared to a post-chemical coating [22]. The mechanism by which cation substitutions improve the electrochemical performance remains a subject of debate. Arunkumar [20] attributed the superior properties of the metal doped-LMN to the smaller parameter differences among the three cubic phases formed during the charge/discharge process, whereas Park et al. [21] reported that Cr doping ($y = 0.05$) provided a wider plateau during charge/discharge tests by suppressing the Mn^{3+} oxidation, thus increasing the structural stability by reduction of the Jahn—Teller distortion. In addition, Liu et al. [22] investigated the Fe substitution for Ni and Mn and found that the superior electrochemical performance of the Fe-substituted LMN is due to the stabilization of a cation-disordered structure, surface enrichment by Fe, suppression of the formation of thick solid-electrolyte interphase (SEI) layers, and much lower polarization resistance due to low charge transfer resistance and diffusion resistance. Meanwhile, Zhong et al. [23] compared the Co, Fe and Cr substitution and confirmed that the transition-metal doping can increase the electronic conductivity, leading to an improvement in the rate capability. In our previous work [24], we have argued that the dopant trivalent Cr^{3+} ions segregate to the surface during synthesis to reduce the concentration of surface Ni^{2+} ions and that the surface high oxidation state Ni^{3+} and Ni^{4+} ions are responsible for oxidation of the electrolyte. Similarly, Shin et al. [25] also proved the segregation of the inert trivalent Ga^{3+} ions to the surface during the synthesis process, providing a robust, more stable interface with the electrolyte at the high operating voltage ($\sim$4.7 V), along with the stabilization of the spinel structure with enhanced disorder of the cations in the octahedral sites.

Whereas much effort has been devoted to study the influence of metal doping ions, only little investigation has been carried out to compare the phase changes with different metal substitutions during lithium de-intercalation/intercalation. We recently demonstrated the phase evolution upon cycling both on a commercial LMN and Cr-doped LMN using in-situ X-ray diffraction (XRD) techniques [26]. The phase diagram for both samples showed the existence of three phases that form alternatively solid solutions and two-phase regions. The analysis of the phase diagram also suggested the faster dynamics of the Li-insertion/de-insertion in the Cr-doped sample, evidenced by the improved capacity retention at high C rates. In this work, we present a comparative in-situ XRD studies of the phase evolution in M-doped LMN cathodes that we shall name in the following M-LMN with M = Co, Al, Cu and Mg in concentration 0.1 per chemical formula.

2. Experimental

In this study, all the M-LMN samples were synthesized by a post-annealing method as described in our earlier work [27], i.e. stoichiometric amounts of lithium, nickel, manganese acetates and cobalt acetate (99% Aldrich) or magnesium (aluminum, copper) nitrate (99% Aldrich) were dissolved and precipitated by adding oxalic acid solution, followed by pre-firing the precursors at 500 °C for 6 h and then another 12 h at 800 °C. After grinding, the black powders were post-annealed for 48 h at 600 °C to get the final samples.

To prepare the cathode films, the cathode powders were made into slurries with $\sim$89 wt.% active material, 6wt.% conductive carbon and 5 wt.% of PVDF binder. The slurries were coated on a 15-μm thick aluminum foil and then dried, cut into 19 mm disks. The in-situ XRD patterns were collected from a standard 2032 coin cell (as depicted in Ref. [26]) in which a 15-μm thick Al foil was used as window for the XRD beam and current collector for the cathode. A 10 mm hole was drilled on the top case of the cell for the X-ray to pass through. A cathode film was put into the case with the aluminum collector facing the hole. Silver epoxy was used to seal the top case with aluminum. The in-situ X-ray measurement was performed on a Bruker D8 Advance diffractometer with Cu-Kα radiation. The data were collected every 2 h with scan-step size 0.025°. The sample displacements were corrected by taking aluminum diffraction peaks as reference. The as-made films were also characterized by X-ray diffraction, with same step size but longer data-collect time in order to collect all the peaks, especially the weak ones.

The electrochemical cells consist of a M-LMN cathode, a separator (Celgard 3501), a Li counter electrode and electrolyte which is a mixture of 1 mol L^{-1} $LiPF_6$ dissolved in ethylene carbonate—dimethyl carbonate (1:1 v/v). All the components were dried at 80—120 °C overnight under vacuum and then assembled in an argon-filled glove box. The electrochemical measurements were carried out on Biologic SP300 (BioLogic Science Instrument), controlled by EC-Lab (V10.19), between 3.5 and 4.9 V. The experimental coin-cells were first cycled at C/12 rate to activate the cathode materials, and then cycled at lower rate of C/24, where all the XRD data were collected.

3. Results and discussion

3.1. Structural analyses of the electrode films

First, one has to determine the chemical formula of the different samples, which amounts to determine whether the dopant substitutes for Mn or Ni, which we may infer from the consideration of ionic radii. Co^{3+} and Cr^{3+} ions in the coordination VI have almost the same radius $r = 0.61$ and 0.615 Å, respectively. On another hand, $r(Ni^{2+}) = 0.69$ Å, and $r(Mn^{4+}) = 0.53$ Å, so that $2r(Co^{3+}) \sim 2r(Cr^{3+}) \sim r(Mn^{4+}) + r(Ni^{2+})$. Therefore, the ionic radius of these two dopants is the ideal value that permits the substitution of one Mn^{4+} ion and one Ni^{2+} ion by two Co^{3+} or two Cr^{3+} ions with the minimum local strain and deformation while keeping the charge neutrality. This scheme has been verified at least in the case of chromium, since the Cr^{3+} ions form antiferromagnetic Cr^{3+}—Cr^{3+} dimers in this spinel compound [27]. Note that this is also the reason why we have assumed that Co^{3+} is in the high

Table 1
Results of the Rietveld refinement of the XRD data for the as-prepared samples, according to the space group *Fdm* corresponding to the disordered spinel phase. The lattice parameter and cell volume for the undoped sample prepared under the same conditions are from Ref. [24], and are also reported here for comparison.

Sample	Lattice parameter (Å)	Cell volume ($Å$)^3	R_{wp} (%)
$LiMn_{1.5}Ni_{0.5}O_4$	8.1763(3)	546.60	0.92
$LiMn_{1.45}Ni_{0.45}Co_{0.1}O_4$	8.1663(3)	544.61	0.96
$LiMn_{1.4}Ni_{0.5}Al_{0.1}O_4$	8.1598(9)	543.32	2.07
$LiMn_{1.5}Ni_{0.4}Cu_{0.1}O_4$	8.1730(1)	545.95	1.57
$LiMn_{1.5}Ni_{0.4}Mg_{0.1}O_4$	8.1708(6)	545.50	2.00
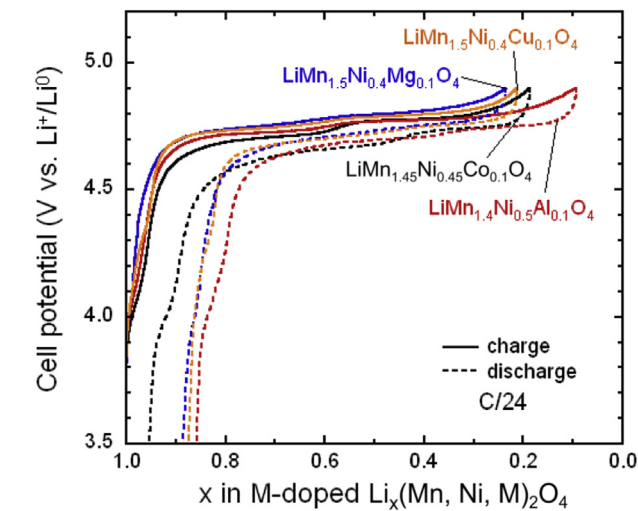
Fig. 1. Charge/discharge curves of the different metal ions-doped LMN at C/24 rate.

Table 2
The voltage difference ΔV, between two anodic peaks, in the different LMN samples.

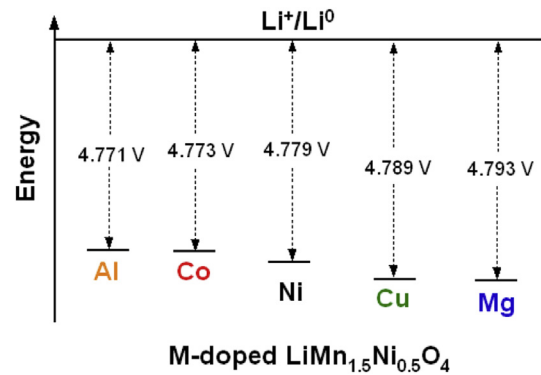| Cathode	Undoped-LMN	Co-LMN	Al-LMN	Cu-LMN	Mg-LMN
ΔV (mV)	29	63	49	46	40

Fig. 3. Positions of the Ni^{2+}/Ni^{4+} redox energies relative to that of Li^+/Li^0 in metal-doped cathodes and the effect of substitutions on the cell voltage.

spin state since the ionic radius in the low-spin state is smaller (0.545 Å), which would imply both a larger local deformation to accommodate the difference in lattice parameter, and a larger crystal field potential, these two effects adding to increase the
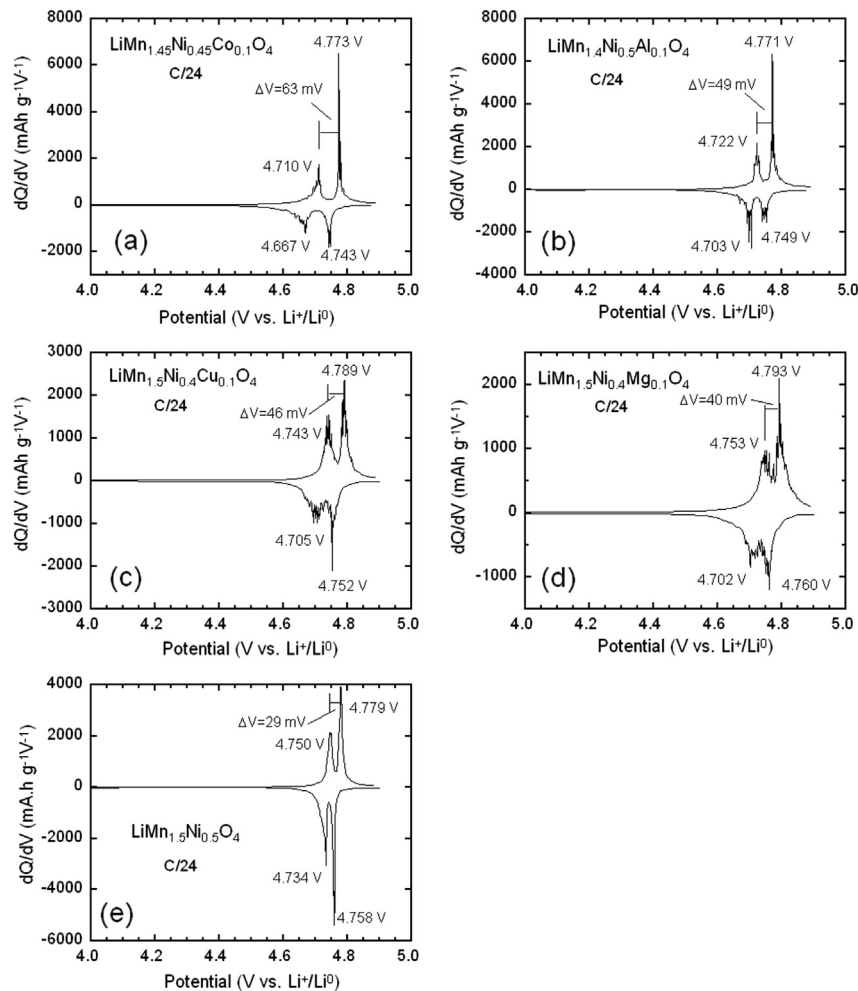

Fig. 2. Differential capacity curves, dQ/dV vs. V, of the (a) Co-LMN (b) Al-LMN (c) Cu-LMN and (d) Mg-LMN cathodes. (e) undoped-LMN is also shown as reference.

formation energy. As a consequence, the chemical formula for the Cr- and the Co-doped sample can be written: $LiMn_{1.45}Ni_{0.45}(Co,Cr)_{0.1}O_4$. This discussion let us expect that the electrochemical properties of the Cr-doped and Co-doped LMN give basically the same results. As we shall see here under, this is indeed what we observed.

On another hand, aluminum is necessarily trivalent with $r(Al^{3+}) = 0.535$ Å, too small with respect to the 'ideal' value 0.61 Å met in the case of Cr or Co-doping. Actually, $r(Al^{3+})$ is close to $r(Mn^{4+})$, which suggests that Al^{3+} substitutes for Mn^{4+}. In that case, the charge neutrality could be recovered by promoting the nearest Ni neighbor to the Ni^{3+} state. Then, the chemical formula is $LiMn_{1.4}Ni_{0.5}Al_{0.1}O_4$ or, to be more specific, $LiMn^{4+}_{1.4}Ni^{2+}_{0.4}Ni^{3+}_{0.1}Al^{3+}_{0.1}O_4$.

The magnesium is necessary divalent and its ionic radius is comparable with that Ni^{2+}, for which it must then substitute, so that the chemical formula is $LiMn_{1.5}Ni_{0.4}Mg_{0.1}O_4$, and all the nickel ions are in the divalent state, while all the Mn ions are in the tetravalent state.

The case of Cu is more ambiguous, because it can be either in the Cu^{2+} state, in which case $r(Cu^{2+}) = 0.73$ Å and it can substitute for Ni^{2+} without any charge compensation, or it can be in the trivalent state with $r(Cu^{3+}) = 0.54$ Å and substitute for Mn^{4+}. Since, however, this would require a charge compensation like in the case of Al-doping, the fundamental state should rather be Cu^{2+} on a Ni^{2+} state, corresponding to the formula $LiMn_{1.5}Ni_{0.4}Cu_{0.1}O_4$.

To identify the crystallographic phase, we performed XRD analysis on the as-prepared cathode films. The results of the
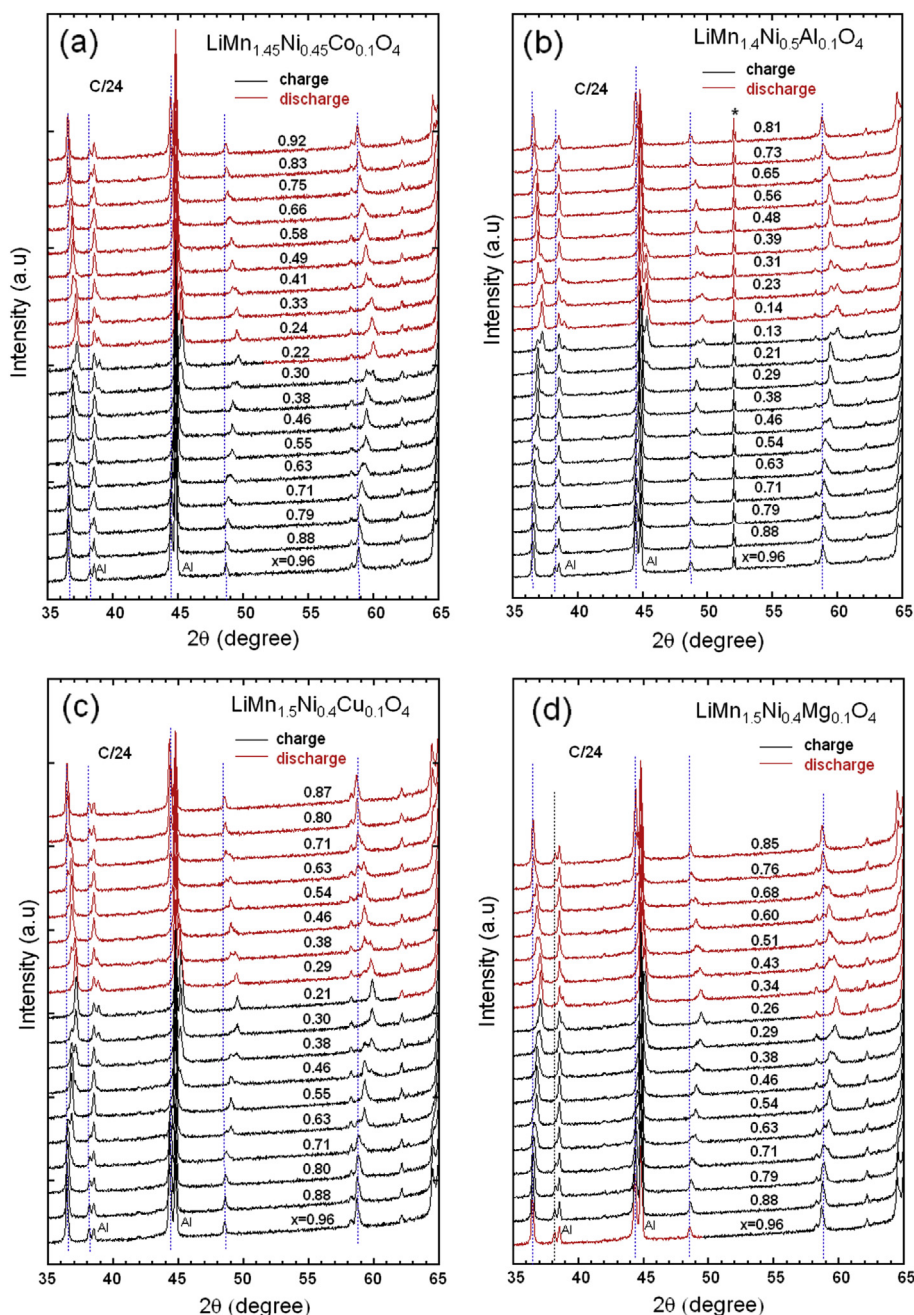

Fig. 4. In-situ XRD patterns (a) Co-LMN, (b) Al-LMN, (c) Cu-LMN and (d) Mg-LMN as a function of the Li-concentration x during the galvanostatic cycling.

Rietveld refinement of the XRD data in the space group *Fdm* (JCPDS No. 80-2162) of the long-range disordered cubic spinel are reported in Table 1. No detective superstructure peaks indicative of an ordering of the Ni(II) and Mn(IV) ions in the $P4_332$ spinel structure [19] was observed in this work. Lafont [28] and Oh [29] et al. reported that a long-range ordered spinel was obtained with Mg and Al substitutions, which can be ascribed to the different annealing temperatures and procedures. From Rietveld refinement, the lattice parameter varies with different substitutions, which is mainly due to the different dopant ionic radii.

3.2. Charge–discharge curves

Fig. 1 shows the typical charge/discharge curves of the nominal M-LMN samples performed at a low current density of C/24 rate. Two distinct plateaus at around 4.7 V are found for all the cathodes,

indicating of the cation disordering at the octahedral sites. Otherwise, no much difference can be observed from Fig. 1 despite different columbic efficiencies. We note that, according to the formula $Li_xMn_{1.45}Ni_{0.45}Co_{0.1}O_4$, the conversion of the 0.45 Ni^{2+} to the tetravalent state is achieved for a Li concentration $x = 0.1$, which is smaller than the concentration $x = 0.18$ observed at the end of charge. This is in agreement with our previous result according to which, event at C/24 rate, the thermodynamic equilibrium is not reached at the end of charge [26]. On another hand, the conversion of all the Ni ions in to the Ni^{4+} state in $LiMn^{4+}_{1.4}Ni^{2+}_{0.4}Ni^{3+}_{0.1}Al^{3+}_{0.1}O_4$ can be achieved upon removing 0.9 Li per formula, so that the minimum lithium concentration at the end of charge is $x = 0.1$, which is actually in agreement with the experiment. Such is also the case in $LiMn_{1.5}Ni_{0.4}Mg_{0.1}O_4$, and $LiMn_{1.5}Ni_{0.4}Cu_{0.1}O_4$, since the conversion of 0.4 Ni^{2+} in Ni^{4+} is achieved for $x = 0.2$, in reasonable agreement with the result in Fig. 1.
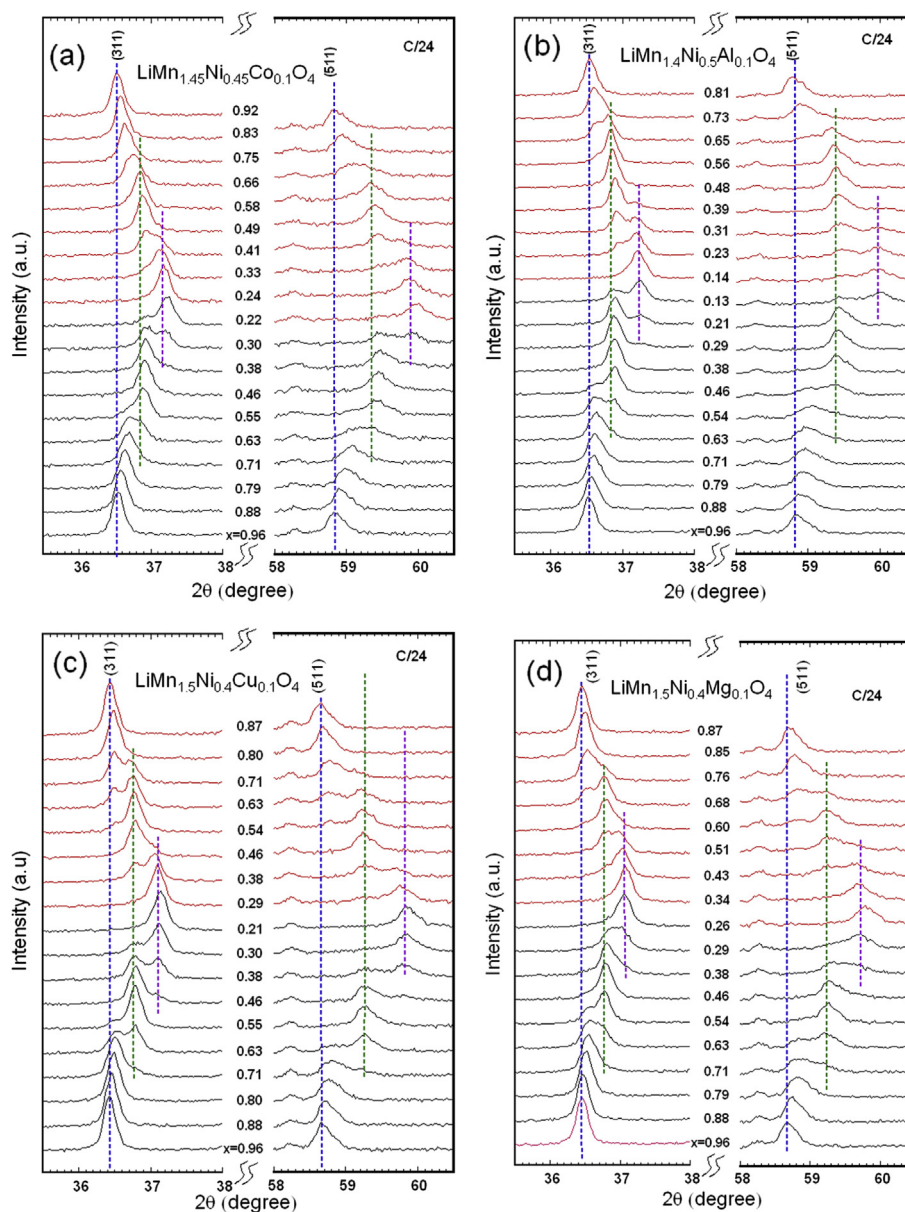
Fig. 5. Selected in-situ XRD patterns of the (311) and (511) peaks for the (a) Co-LMN, (b) Al-LMN, (c) Cu-LMN and (d) Mg-LMN spinels during cycling at C/24 rate. The dotted lines are drawn for the guidance of eyes to view the three different phases, in blue, green and purple for the phases 1, 2, 3, respectively on the web version. (For interpretation of the references to colour in this figure legend, the reader is referred to the web version of this article.)

The related differential capacity curves, dQ/dV vs. V, that provide us with more details are reported in Fig. 2(a)–(d). The differential curves of the undoped-LMN were also shown in Fig. 2(e) as reference. Firstly, all the cathodes show two separated anodic and cathodic peaks in Fig. 2, corresponding to the two voltage plateaus of the charge/discharge curves in Fig. 1. Meanwhile, the potential differences (ΔV) between those two anodic peaks were calculated and summarized in Table 2, from which one can see that ΔV varies with different dopant ions in the spinel cathodes. For instance, Co-LMN gives a larger ΔV of 63 mV, whereas ΔV is smaller for Al, Cu and Mg-doped materials. But they are all larger than that of undoped-LMN: 29 mV. In our previous work [18] we demonstrated that the voltage gap between the two voltage plateaus depends on the degree of ordering; it becomes narrower ($\Delta V = 20$ mV) for the undoped phase while $\Delta V = 60$ mV for Cr-doped spinel. Kunduraci et al. also reported that larger ΔV was observed in the disordered LMN compared with the ordered one [30]. Therefore, the calculated potential difference ΔV in Fig. 2 and Table 1 implies that all the metal substitutions in the present work could increase the cation disorder after high-temperature annealing at 900 °C, especially for the Co-substitution, for which the result is similar to the Cr-substitution.

Further observation in Fig. 2 shows that both anodic and cathodic peaks have different shifts with various substitutions. For example, while the Co-LMN presents two lower anodic peaks at 4.710 and 4.773 V, respectively, two comparably higher anodic peaks at 4.753 and 4.793 V are observed in the Mg-LMN case. For the Al and Cu-doped LMN, the anodic peaks are between those of Co-LMN and Mg-LMN. A similar increase of the voltage shift was reported in the Mg-doped LMN [31], whereas a smaller one was observed in the Co-doped LMN [32]. The voltage variation implies that the host Ni^{2+}/Ni^{4+} redox energy is affected by the nearest neighbor ionic environment. Kim et al. [33] have pointed out that the lithium ions require more energy to be intercalated/de-intercalated from the host structure of ordered LMN, leading to a higher redox potential. Recently, we also reported that Cr-substitution increases the degree of disorder at the octahedral sites compared with the undoped LMN, which results in lowering the voltage by ~30 mV [26–27]. On the other hand, it is known

that the relative positions of the redox energies depend on the nature of the counter cations for an isostructural series of metal-doped olivine phosphates [34] or Ti-doped spinel LMN [35]. In this work, the partial substitution of the more electropositive Co for Ni not only introduces greater disorder of the B-site cations in the spinel LMN, but also increases the Ni–O covalence due to the inductive effect, thereby raises the Ni^{2+}/Ni^{4+} redox energy and consequently decreases the voltage of the Ni^{2+}/Ni^{4+} couple; on another hand, the substitution of a less electropositive Cu for Ni decreases the Ni–O covalence, therefore lowers the Ni^{2+}/Ni^{4+} redox energy and thus increases the voltage of the Ni^{2+}/Ni^{4+} couple (as illustrated in Fig. 3).

In the cases of Mg- and Al-doped LMN, however, the voltage variations cannot be explained by considering the changes in the electronegativity of dopant ions, since the substitution of the more electropositive Mg for Ni would be expected to increase the Ni–O covalence, thereby to raise the Ni^{2+}/Ni^{4+} redox energy, resulting in decline of the voltage of the Ni^{2+}/Ni^{4+} couple. Similarly, if the less electropositive Al would substitute for Ni, then an increase of the voltage of the Ni^{2+}/Ni^{4+} couple would be observed. However, Fig. 3 shows the opposite. This is another evidence that the Al^{3+} ions substitutes for Mn and not Ni, as explained above. Therefore, one can conclude that in the metal-doped spinel LMN, the redox reaction potentials are sensitive to the cation ordering and the electronegativity of the neighboring metal ions as well as the radii of the dopants. Note the excellent weighted powder profile R-parameter (R_{wp}) also reported in Table 1 corroborates the accuracy of the substitutions we have proposed, which are also the substitutions that minimize this parameter.

3.3. Phase evolution during the electrochemical process

We recently compared the phase evolution between undoped and Cr-doped LMN by using in-situ XRD techniques [26]. In this work, we thus mainly focus attention on the phase diagrams of the Co, Al, Cu and Mg-substituted LMN, while undoped and Cr-doped LMN will only be mentioned and we refer to [26] for further discussion.
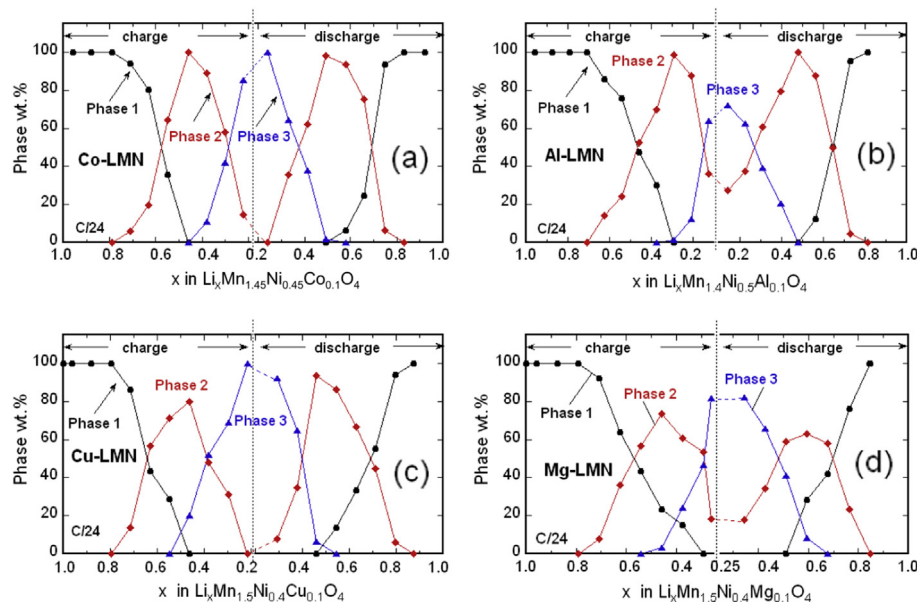
Fig. 6. Relative concentrations of the different cubic phases in (a) Co-LMN, (b) Al-LMN, (c) Cu-LMN and (d) Mg-LMN samples as a function of the Li concentration x during a cycle at C/24 rate.
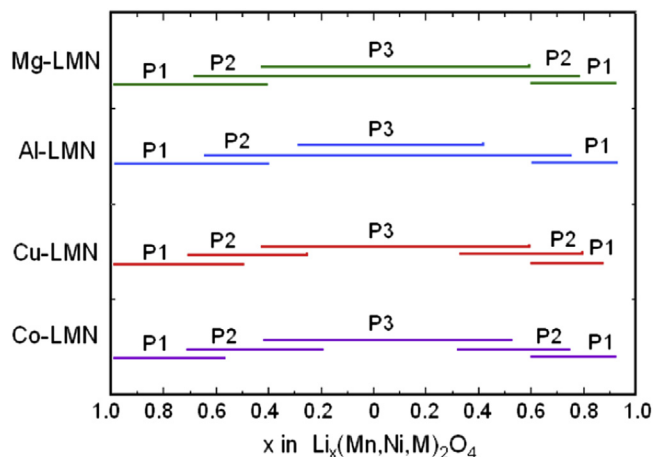
Fig. 7. Comparison of the different cubic phase diagrams in different metal-doped LMN cathodes as a function of Li concentration x during a cycle at C/24 rate.

Fig. 4 shows the evolution of in-situ XRD patterns of the four doped-LMN electrode films during cycling at C/24 rate. Similarly to our previous work [26], two diffraction peaks, i.e. (311) in the range $2\theta = 35.5-38°$ and (511) in the range $2\theta = 58-60.5°$ had the minimum overlap with the Bragg line of the Al current collector, the reason why have been selected to better study the phase change. Fig. 5 presents the evolution of these (311) and (511) diffraction peaks in the four LMN spinels during the first charge/discharge process. In general, the phase diagrams for all the spinel samples are qualitatively the same, i.e. all the diffraction peaks shift to higher 2θ angles during the delithiation reaction, and back to lower 2θ angles during the lithiation. Three distinctive cubic phases are successively observed in all the spinels. Assuming that each phase is correlated with different oxidation state of nickel ions, then the phases represented by Ni^{2+}, Ni^{3+}, and Ni^{4+} are located at low, medium, and high diffraction angles, respectively. Firstly, removal of Li from the spinel LMN framework probes the oxidation reaction of Ni^{2+}/Ni^{3+} at the early charge stage where only a solid solution (phase-1) is found. In this process, extraction of Li results only in the shift of diffraction peaks to higher 2θ angles. As charge process

continues, a new cubic spinel phase (phase-2) start to emerge and the system thus enters into a two-phase domain, in which the phase-2 grows at the expense of the phase-1 until the phase-1 disappears. Further delithiation leads the system to another two-phase region with the coexistence of phase-2 and a new phase (phase-3) that grows at the expense of phase-2 until the end of charge. Upon discharge, these processes take place in reverse order.

Although very similar phase changes can be seen in Figs. 4 and 5, there are still some minor differences in the phase evolution among all the spinel samples. In order to better observe those differences, Fig. 6 gives the relative concentrations of the different cubic phases in the doped spinels and the corresponding proportion of each phase as a function of x during the full cycle is also compared in Fig. 7. As can be seen from Figs. 6 and 7, all these three phases emerge and end at different depths of charge/discharge stage with various substitutions. For example, as charge proceeds from $x = 1$, phase-1 is observed in the range of $1 \leq x \leq 0.55$ for Co-LMN and Cu-LMN, whereas the phase-1 is found in the range of $1 \leq x \leq 0.38$ for Al-LMN and Mg-LMN. In addition, phase-2 starts to emerge from $x \geq 0.71$ for Co-LMN, Cu-LMN and Mg-LMN, while for the Al-LMN, phase-2 is found after $x \geq 0.63$. More importantly, no phase-2 can be found from Fig. 7 in the Cu-LMN at the end of charge. In the case of Co-LMN, the small amount of the phase-2 at the end of charge can be attributed to non-equilibrium effects, because at the beginning of discharge, this phase 2 is no longer observed. In contrast, still detectable amount of phase-2 co-exists with phase-3 at the end of charge in Al- and Mg-doped LMN cathodes, a situation close to that of the undoped-LMN as shown in Fig. 8, which is probably due to the out-of-equilibrium effects [26]. It is indeed possible that the lithium distribution has been frozen in an out-of-equilibrium state in these two cases. At the beginning of the charge, the proportion of the phase-2 has been decreases only slightly, and in the case of Mg-doping, the proportion at the end of charge and at the beginning of the discharge are the same. Similar evolution was also found in cation-ordered LMN [36], where even three cubic phases co-existed at the end of charge due to the kinetic limitation of lithium extraction from the ordered LMN. However, all the substituted-LMN cathodes show the same long-range disordered structures in this work. Therefore, the degree of cation ordering is not the only parameter that affects the phase diagram and other parameters such as the out-of-equilibrium effects and the
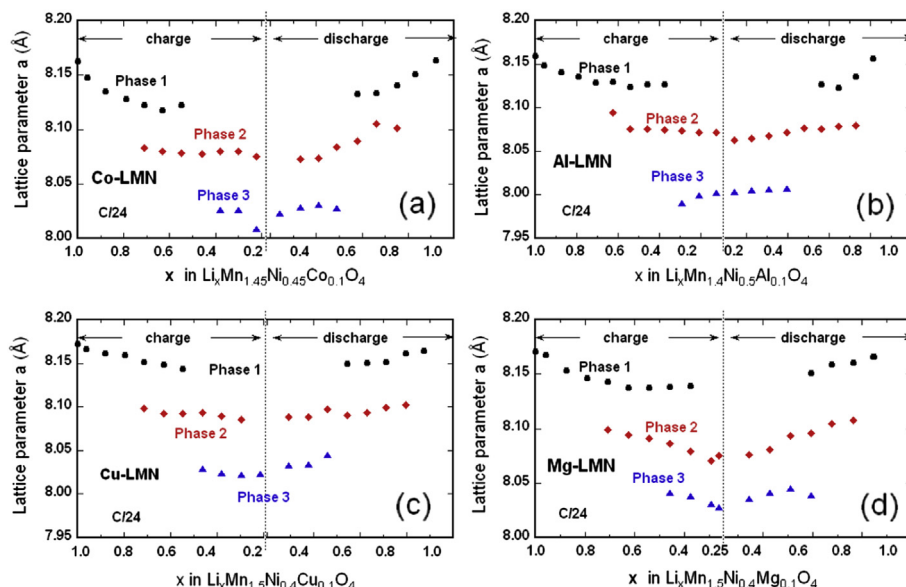

Fig. 8. Variation of the lattice parameters as a function of the Li concentration x during the charge/discharge in (a) Co-LMN, (b) Al-LMN, (c) Cu-LMN and (d) Mg-LMN cathodes.

morphology of the particles [37] must be taken into consideration. In this work, we can invoke the high level of metal substitutions that may lead some of the non-transition metal dopant Al and Mg ions to occupy the tetrahedral 8a sites in these cathodes as found in Al-substituted spinel LiMn$_2$O$_4$ [38] and Al-, Mg-substituted LMN [39], due to the 3d^0 configuration with no crystal field stabilization energy. Consequently, equal amounts of Li ions may migrate to the octahedral 16d sites. In the spinel LMN, generally, Li at tetrahedral 8a site moves to vacant octahedral 16c site, the 3-D 8a–16c–8a–16c network provides an energetically favorable pathway for the rapid diffusion of lithium in and out of the structure during discharge and charge, respectively. However, the occupancy of Al or Mg ions at tetrahedral 8a sites makes it hard to extract the inactive lithium ions at 16d sites out of the host structure, leaving trace of

Ni^{3+} remained (phase-2) at the end of charge process, despite the long-range disordered spinel structure. On the contrary, most of the transition-metal ions Co and Cu may randomly locate at the octahedral 16d site, thus increasing the disordering distribution as well as the electronic conductivity [12,20,23]. This hypothesis also provides an explanation for the better electrochemical properties of the Co-LMN and Cu-LMN electrodes compared with the non-transition metal-doped Al-LMN and Mg-LMN, especially at higher C-rates (Fig. 9a). It is also necessary to note that the phase evolution of Co-LMN is very close to that of Cr-LMN (see Fig. 6 in Ref. [26]), hence, similarly improved electrochemical property can be expected for Co-LMN as evidenced in Fig. 9b. However, the poor electrochemical performances of Al-LMN and Mg-LMN in this work are not consistent with the results found for the Al or Mg-substituted LMN in Refs. [28,31]; this is probably due to the fact that lower concentration of Al or Mg doping were used in these prior works.

Moreover, it has been proved that the lattice parameter varies with x for the phase-1 in the Fd$\bar{m}$ case, while it remains almost constant in the P4$_3$32 case [30,33,36], which is consistent with our previous results [27] and other works as well [9,23,30] showing that Cr-substitution increases the disordered structure within the LiMn$_{1.5}$Ni$_{0.5}$O$_4$ spinel lattice. Actually the stronger parameter variation for the phase-1 could be an evidence of the stronger cation disorder in spinel LMN [26]. Analyses of the in-situ XRD patterns from Figs. 4 and 5 show that all the three phases are cubic structures during charge/discharge process. The lattice parameter for each phase was calculated and plotted in Fig. 8(a)–(d), from which the Co-doped case gives the largest parameter variation in phase-1, implying that the Co-substitution introduces the largest disorder of the B-site cations in the spinel LMN. The largest lattice parameter variation of phase-1 with x in the Co-doped LMN is also in agreement with the largest ΔV in Fig. 2 and the best electrochemical property in Fig. 9.

4. Conclusion

In this work, comparative studies of the phase evolution in the nominal LiMn$_{1.5}$Ni$_{0.5}$O$_4$ cathode materials doped with various metal such as Co, Al, Cu, and Mg were carried out by in-situ XRD. It was found that three phases are observed in all the doped cathodes that form alternatively solid solutions and two-phase regions during charge/discharge process. However, each phase emerge and end at different stages with various substitutions. We argued that some of the non-transition metal Al or Mg ions may occupy the tetrahedral 8a sites under high level substitution, displacing equal amounts of Li$^+$ ions into the octahedral 16d sites. The occupancy of octahedral 16d site by trace of inactive lithium plays an important role in the phase evolution, which can be also used to explain the different electrochemical properties. Charge/discharge test also shows a minor but detectable voltage variation of the Ni^{2+}/Ni^{4+} redox couple in the substituted cathodes. This result was understood on a basis of a model that takes both changes in the electronegativity and the radii of the dopant ions into account. The analyses also confirm that substitution of certain amounts of Ni by Co ions introduces the largest cation disordering, which is evidenced by the best electrochemical performance among all the M-doped LiMn$_{1.5}$Ni$_{0.5}$O$_4$ in this work.
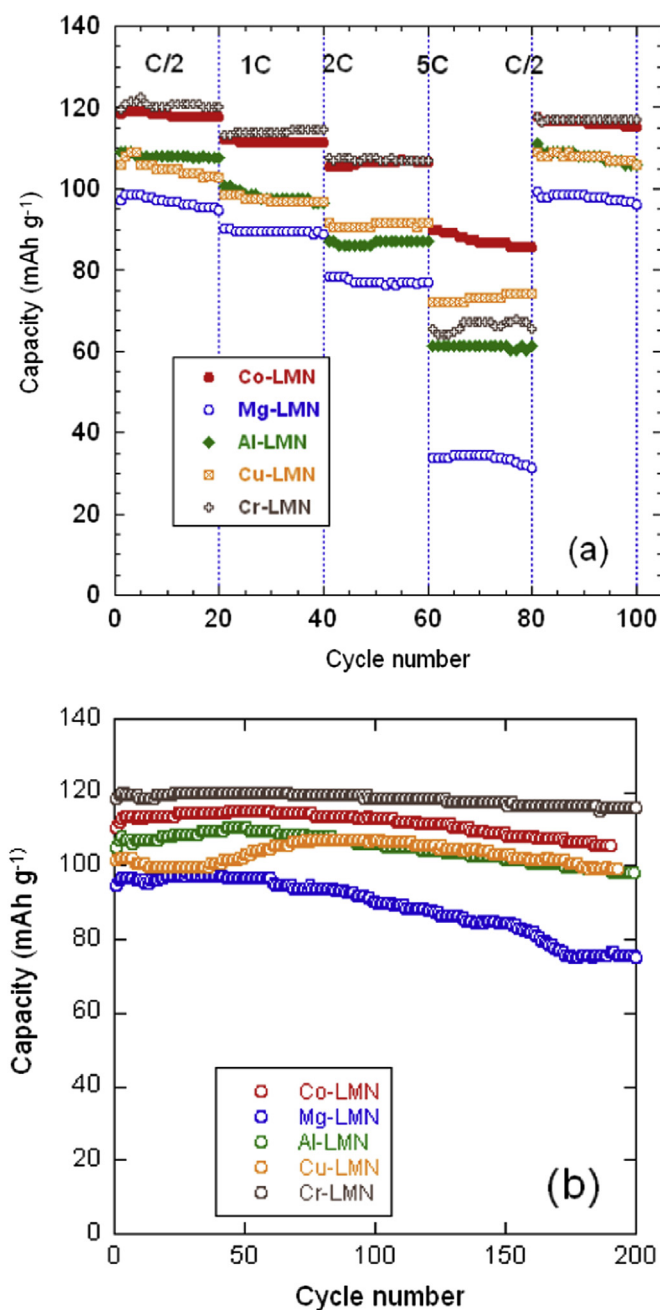
Acknowledgments

Fig. 9. Electrochemical performance of metal-doped LMN cathodes: (a) discharge capacity vs. C-rate and (b) stability of M-LMN/Li cells upon cycling.

References

[1] B. Markovsky, Y. Talyossef, G. Salitra, D. Aurbach, H.-J. Kim, S. Choi, Electrochem. Commun. 6 (2004) 821.
[2] P.G. Bruce, B. Scrosati, J.-M. Tarascon, Angew. Chem. Int. Ed. 47 (2008) 2930.
[3] K. Mitzushima, P.C. Jones, P.J. Wiseman, J.B. Goodenough, Mater. Res. Bull. 15 (2008) 783.
[4] B. Kang, G. Ceder, Nature 458 (2008) 190.
[5] R. Santhanam, B. Rambabu, J. Power Sources 195 (2010) 5442.
[6] T. Yi, Y. Xie, M. Ye, L. Jiang, R. Zhu, Y. Zhu, Ionics 17 (2011) 383.
[7] M. Kunduraci, J.F. Al-Sharab, G.G. Amatucci, Chem. Mater. 18 (2006) 3585.
[8] J. Xiao, X. Chen, P.V. Sushko, M.L. Sushko, L. Kovarik, J. Feng, Z. Deng, J. Zheng, G.L. Graff, Z. Nie, D. Choi, J. Liu, J.-G. Zhang, M.S. Whittingham, Adv. Mater. 24 (2012) 2109.
[9] D.W. Shin, C.A. Bridges, A. Huq, M.P. Paranthaman, A. Manthiram, Chem. Mater. 24 (2012) 3720.
[10] H.-M. Cho, Y.S. Meng, J. Electrochem. Soc. 160 (2013) A1482.
[11] J. Song, D.W. Shin, Y. Lu, C.D. Amos, A. Manthiram, J.B. Goodenough, Chem. Mater. 24 (2012) 3101.
[12] K.R. Chemelewski, A. Manthiram, J. Phys. Chem. C 117 (2013) 12465.
[13] Y.K. Sun, Y.S. Li, M. Yoshio, K. Amine, Electrochem. Solid State Lett. 5 (2002) A99.
[14] Y.-K. Sun, K.-J. Hong, J. Prakash, K. Amine, Electrochem. Commun. 4 (2002) 344.
[15] T. Noguchi, I. Yamazaki, T. Numata, M. Shirakata, J. Power Sources 174 (2007) 359.
[16] J. Liu, A. Manthiram, Chem. Mater. 21 (2009) 1695.
[17] H.M. Wu, I. Belharouak, A. Abouimrane, Y.-K. Sun, K. Amine, J. Power Sources 195 (2010) 2909.
[18] D. Liu, J. Trottier, P. Charest, J. Fréchette, A. Guerfi, A. Mauger, C.M. Julien, K. Zaghib, J. Power Sources 204 (2010) 127.
[19] R. Alcantara, M. Jaraba, P. Lavela, J.L. Tirado, Chem. Mater. 15 (2003) 2376.
[20] T.A. Arunkumar, A. Manthiram, Electrochem. Solid State Lett. 8 (2005) A403.
[21] S.B. Park, W.S. Eom, W.I. Cho, H. Jang, J. Power Sources 159 (2006) 679.
[22] J. Liu, A. Manthiram, J. Phys. Chem. C 113 (2009) 15073.
[23] G.B. Zhong, Y.Y. Wang, Y.Q. Yu, C.H. Chen, J. Power Sources 205 (2012) 385.
[24] D. Liu, Y. Lu, J.B. Goodenough, J. Electrochem. Soc. 157 (2010) A1269.
[25] D.W. Shin, A. Manthiram, Electrochem. Commun. 13 (2011) 1213.
[26] W. Zhu, D. Liu, J. Trottier, C. Gagnon, A. Mauger, C.M. Julien, K. Zaghib, J. Power Sources 242 (2013) 236.
[27] D. Liu, J. Hamel-Paquet, J. Trottier, F. Barray, V. Gariépy, P. Hovington, A. Guerfi, A. Mauger, C.M. Julien, J.B. Goodenough, K. Zaghib, J. Power Sources 217 (2012) 400.
[28] U. Lafont, C. Locati, W.J.H. Borghols, A. Łasinska, J. Dygas, A.V. Chadwick, E.M. Keldera, J. Power Sources 189 (2009) 179.
[29] S.H. Oh, K.Y. Chung, S.H. Jeon, C.S. Kim, W.I. Cho, B.W. Cho, J. Alloys Compd. 469 (2009) 244.
[30] M. Kunduraci, G.G. Amatucci, J. Electrochem. Soc. 153 (2006) A1345.
[31] F.G.B. Ooms, E.M. Kelder, J. Schoonman, M. Wagemaker, F.M. Mulder, Solid State Ionics 152 (2002) 143.
[32] A. Ito, D. Li, Y. Lee, K. Kobayakawa, Y. Sato, J. Power Sources 185 (2008) 1249.
[33] J.-H. Kim, S.-T. Myung, C.S. Yoon, S.G. Kang, Y.-K. Sun, Chem. Mater. 16 (2004) 906.
[34] G. Kobayashi, A. Yamada, S. Nishimura, R. Kannoa, Y. Kobayashi, S. Seki, Y. Ohno, H. Miyashiro, J. Power Sources 189 (2009) 397.
[35] J.-H. Kim, S.-T. Myung, C.S. Yoon, I.-H. Oh, Y.-K. Sun, J. Electrochem. Soc. 151 (2004) A1911.
[36] L. Wang, H. Li, X. Huang, E. Baudrin, Solid State Ionics 193 (2011) 32.
[37] B. Hai, A.K. Shukla, H. Duncan, G. Chen, J. Mater. Chem. A 1 (2013) 759.
[38] J.-S. Kim, J.T. Vaughey, C.S. Johnson, M.M. Thackeray, J. Electrochem. Soc. 150 (2003) A1498.
[39] G.T.-K. Fey, C.-Z. Lu, T.P. Kumar, J. Power Sources 115 (2003) 332.